

Axion searches with the EDELWEISS-II experiment

E. Armengaud,^a Q. Arnaud,^b C. Augier,^b A. Benoit,^c A. Benoit,^b L. Bergé,^d T. Bergmann,^e J. Blümer,^{f,g} A. Broniatowski,^d V. Brudanin,^h P. Camus,^c A. Cazes,^b B. Censier,^b M. Chapellier,^d F. Charlieux,^b F. Couëdo,^d P. Coulter,ⁱ G.A. Cox,^f T. de Boissière,^a M. De Jesus,^b Y. Dolgorouky,^d A.A. Drillien,^d L. Dumoulin,^d K. Eitel,^g D. Filosofov,^h N. Fourches,^a J. Gascon,^b G. Gerbier,^a M. Gros,^a L. Hehn,^g S. Henry,ⁱ S. Hervé,^a G. Heuermann,^f N. Holtzer,^d V. Humbert,^d A. Juillard,^b C. Kéfélian,^{b,f} M. Kleifges,^e H. Kluck,^f V. Kozlov,^g H. Kraus,ⁱ V.A. Kudryavtsev,^j H. Le Sueur,^d M. Mancuso,^d C. Marrache-Kikuchi,^d S. Marnieros,^d A. Menshikov,^e X-F. Navick,^a C. Nones,^a E. Olivieri,^d P. Pari,^k B. Paul,^a M.C. Piro,^{a,d} O. Rigaut,^d M. Robinson,^j S. Rozov,^h V. Sanglard,^b B. Schmidt,^f B. Siebenborn,^g D. Tcherniakhovski,^e M. Tenconi,^d L. Vagneron,^b R.J. Walker,^g M. Weber,^e E. Yakushev,^h X. Zhangⁱ
(The EDELWEISS Collaboration)

^aCEA, Centre d'Etudes Saclay, IRFU, 91191 Gif-Sur-Yvette Cedex, France

^bIPNL, Université de Lyon, Université Lyon 1, CNRS/IN2P3, 4 rue E. Fermi 69622 Villeurbanne cedex, France

^cCNRS-Néel, 25 Avenue des Martyrs, 38042 Grenoble cedex 9, France

^dCSNSM, Université Paris-Sud, IN2P3-CNRS, bat 108, 91405 Orsay, France

^eKarlsruhe Institute of Technology, Institut für Prozessdatenverarbeitung und Elektronik, 76021 Karlsruhe, Germany

^fKarlsruhe Institute of Technology, Institut für Experimentelle Kernphysik, 76128 Karlsruhe, Germany

^gKarlsruhe Institute of Technology, Institut für Kernphysik, 76021 Karlsruhe, Germany

^hLaboratory of Nuclear Problems, JINR, Joliot-Curie 6, 141980 Dubna, Moscow region, Russia

ⁱUniversity of Oxford, Department of Physics, Keble Road, Oxford OX1 3RH, UK

^jDepartment of Physics and Astronomy, University of Sheffield, Hounsfield Road, Sheffield S3 7RH, UK

^kCEA, Centre d'Etudes Saclay, IRAMIS, 91191 Gif-Sur-Yvette Cedex, France

E-mail: claudia.nones@cea.fr, thibault.main-de-boissiere@cea.fr,
eric.armengaud@cea.fr

Abstract. We present new constraints on the couplings of axions and more generic axion-like particles using data from the EDELWEISS-II experiment. The EDELWEISS experiment, located at the Underground Laboratory of Modane, primarily aims at the direct detection of WIMPs using germanium bolometers. It is also sensitive to the low-energy electron recoils that would be induced by solar or dark matter axions. Using a total exposure of up to 448 kg.d, we searched for axion-induced electron recoils down to 2.5 keV within four scenarios involving different hypotheses on the origin and couplings of axions. We set a 95 % CL limit on the coupling to photons $g_{A\gamma} < 2.13 \times 10^{-9} \text{ GeV}^{-1}$ in a mass range not fully covered by axion helioscopes. We also constrain the coupling to electrons, $g_{Ae} < 2.56 \times 10^{-11}$, similar to the more indirect solar neutrino bound. Finally we place a limit on $g_{Ae} \times g_{AN}^{\text{eff}} < 4.70 \times 10^{-17}$, where g_{AN}^{eff} is the effective axion-nucleon coupling for ^{57}Fe . Combining these results we fully exclude the mass range $0.91 \text{ eV} < m_A < 80 \text{ keV}$ for DFSZ axions and $5.73 \text{ eV} < m_A < 40 \text{ keV}$ for KSVZ axions.

Contents

1	Introduction	1
2	Possible axion sources: the Sun and the galactic halo	2
2.1	Axion production in the Sun	2
2.1.1	Production by Primakoff effect	3
2.1.2	Production via ^{57}Fe nuclear magnetic transition	4
2.1.3	Compton, bremsstrahlung and axio-RD processes	6
2.2	Axions as dark matter	7
3	Axion interactions in EDELWEISS detectors	7
4	EDELWEISS-II data and backgrounds	8
5	Axion search: Primakoff solar axions	10
6	Axion search: 14.4 keV solar axions	13
7	Axion search: Compton, bremsstrahlung and axio-RD	14
8	Axion search: dark matter axions	15
9	Results and discussion	17
10	Conclusions	20

1 Introduction

Following Peccei and Quinn's original solution [1] to the CP problem in QCD, Weinberg [2] and Wilczek [3] deduced the existence of a new, elusive pseudo-scalar particle, the axion. Both the axion mass and the strength of its couplings to ordinary particles are inversely proportional to the Peccei-Quinn symmetry-breaking scale f_A . While the original axion model with f_A associated with the electroweak scale was quickly dismissed by subsequent experiments, "invisible" axions with f_A as a free parameter are still viable. The most frequently studied are the so-called hadronic models such as KSVZ (Kim-Shifman-Vainstein-Zakharov) [4] and the GUT models such as the DFSZ (Dine-Fischler-Srednicki-Zhitnitskii) model [5]. These models still provide a solution to the strong CP problem. In both cases, the axion mass, m_A , is related to f_A :

$$m_A = \left[\frac{z}{(1+z+w)(1+z)} \right]^{\frac{1}{2}} \frac{f_\pi m_\pi}{f_A} = 6 \text{ eV} \times \left(\frac{10^6 \text{ GeV}}{f_A} \right) \quad (1.1)$$

where $m_\pi = 135 \text{ MeV}$ is the pion mass, $f_\pi \approx 92 \text{ MeV}$ the pion decay constant, while $z = m_u/m_d = 0.56$ and $w = m_u/m_s = 0.029$ are the mass ratios of the lightest up, down and strange quarks, with significant uncertainties especially for z [6]. We use $\hbar = c = 1$.

The effective axion couplings to photons ($g_{A\gamma}$), electrons (g_{Ae}) and nucleons (g_{AN}) are model dependent [7, 8]. For example, hadronic axions are coupled to new, heavy quarks

and do not interact with ordinary quarks and leptons at the tree level leading to a strong suppression of g_{Ae} . On the contrary, DFSZ axions require that Standard Model quarks and leptons carry a Peccei-Quinn charge. Experimental searches and astrophysical constraints can be translated to limits on f_A , or equivalently on the axion mass, within a given axion model. On the other hand, axion-like particles (ALPs) are pseudo-scalar fields generically predicted by string theory [9], as the Kaluza-Klein zero modes of anti-symmetric tensor fields. The mass and couplings of ALPs are not directly related to their Peccei-Quinn-like scale. It is therefore relevant to also search for ALP couplings in a model-independent way.

The purpose of this article is to report on a study of the interaction of axions or ALPs produced by different mechanisms in the Sun or constituting the galactic dark matter halo (Section 2) with EDELWEISS-II germanium bolometers operated underground and described in Section 4. Two detection mechanisms in the germanium detectors, described in Section 3, are exploited: the coherent Bragg diffraction, related to $g_{A\gamma}$ and the axio-electric effect, which is the analogue of a photo-electric effect with the absorption of an axion instead of a photon. We benefit from the quality of the EDELWEISS-II data set: a large exposure corresponding to 14-month data taking with ten 400-g germanium detectors, a good energy resolution and a very low background down to an energy threshold of 2.5 keV. This low background was made possible thanks to both the low-radioactivity underground setup of the experiment and the so-called ID detector design [10] which allows a selection of interactions that takes place within a fiducial volume for each detector. We carry out four axion searches associated with different benchmark scenarios. These searches are described in Sections 5-8. The derived constraints on axion couplings will be discussed, and in particular we interpret them within the specific DFSZ and KSVZ axion models.

2 Possible axion sources: the Sun and the galactic halo

The Sun could be a major source of axions. The different mechanisms which can lead to axion production in the Sun will be briefly reviewed in Section 2.1. A second possibility is that axions constitute a major fraction of dark matter and are present in the galactic halo, as described in Section 2.2.

2.1 Axion production in the Sun

Several production mechanisms will be briefly described and considered later for data analysis:

1. Primakoff production: $\gamma \rightarrow A$ in the presence of charged particles
2. Nuclear magnetic transition of ^{57}Fe nuclei: $^{57}\text{Fe}^* \rightarrow ^{57}\text{Fe} + A$
3. Compton-like scattering: $e^- + \gamma \rightarrow e^- + A$
4. Axion bremsstrahlung: $e^- \rightarrow e^- + A$ in the presence of charged particles
5. Axio-recombination: $e^- + I \rightarrow I^- + A$ where I is an ion
6. Axio-deexcitation: $I^* \rightarrow I + A$ where I^* is an excited state of I

We will refer to the sum of axio-recombination and axio-deexcitation as the axio-RD mechanism. The relative intensity of the mechanisms is model-dependent. For example, in the case of non hadronic axions such as those described by the DFSZ model, fluxes related to Compton

and bremsstrahlung processes are far more intense than those predicted by hadronic models for the same value of f_A . This is due to the fact that the coupling to electrons arises at the tree level. In this case, the Compton and bremsstrahlung channels for axion production largely prevail over the Primakoff effect (see Section 5). On the contrary, the latter dominates hadronic axion emission. As for the ^{57}Fe axions, whose flux depends only on the isoscalar and isovector coupling constants, the axion production rate is similar in hadronic and non hadronic models. Fig. 1 shows the evaluated fluxes on Earth for the various processes.

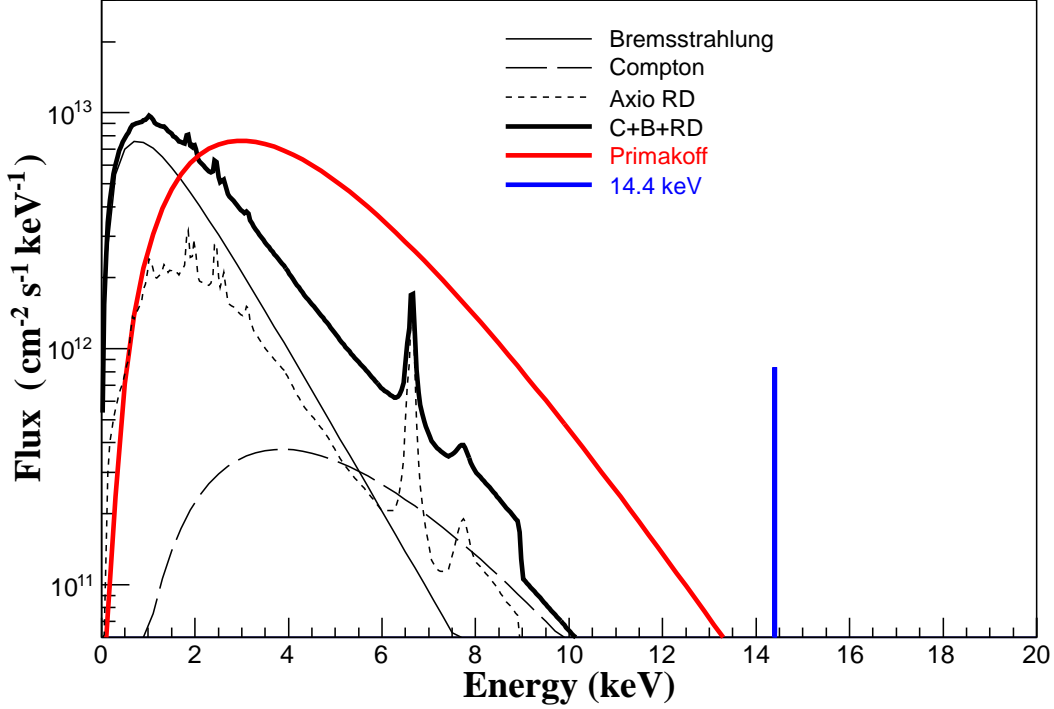


Figure 1. Predicted solar axion fluxes in the EDELWEISS detectors from different mechanisms. The thick solid black line corresponds to the sum of Compton, bremsstrahlung and axio-RD (recombination-deexcitation). Red: Primakoff axions. Blue: ^{57}Fe nuclear transition. The intrinsic width of this line, dominated by Doppler broadening, is 5 eV. The effective axion couplings corresponding to the represented fluxes are $g_{A\gamma} = 10^{-9} \text{ GeV}^{-1}$, $g_{Ae} = 10^{-11}$ and $g_{AN}^{\text{eff}} = 10^{-7}$.

2.1.1 Production by Primakoff effect

Axions could be efficiently produced in the Sun by the inverse Primakoff conversion of thermal photons in the electromagnetic field of the solar plasma. The effective Lagrangian of the axion-photon coupling is given by:

$$\mathcal{L} = -\frac{1}{4}g_{A\gamma}F^{\mu\nu}\tilde{F}_{\mu\nu}\phi_A = g_{A\gamma}\mathbf{E}\cdot\mathbf{B}\phi_A, \quad (2.1)$$

where $F^{\mu\nu}$ is the electromagnetic field tensor, $\tilde{F}_{\mu\nu}$ its dual, ϕ_A the axion field and $g_{A\gamma}$ the axion-photon effective coupling constant.

Within standard axion models, the coupling $g_{A\gamma}$, which has the dimension of $(\text{energy})^{-1}$, can be written as:

$$g_{A\gamma} = \frac{\alpha}{2\pi f_A} \left[\frac{E}{N} - \frac{2(4+z+w)}{3(1+z+w)} \right] \quad (2.2)$$

where α is the fine structure constant and E/N is the ratio of the electromagnetic to color anomalies of the Peccei-Quinn symmetry ($E/N = 8/3$ and 0 for DFSZ and KSVZ models, respectively).

The expected solar Primakoff axion flux was estimated in [11], and is well approximated by the expression where the energy E is in keV:

$$\frac{d\Phi}{dE} = \frac{6.02 \times 10^{14}}{\text{cm}^2 \text{keV s}} \left(\frac{g_{A\gamma} \times 10^8}{\text{GeV}^{-1}} \right)^2 E^{2.481} e^{-E/1.205} \quad (2.3)$$

This corresponds to a broad spectrum, with an average energy of about 4.2 keV and a negligible intensity above 10 keV as shown in Fig. 1. The intensity of the resulting axion flux scales as $g_{A\gamma}^2$. Finally, we mention that this flux estimation is valid for ultra-relativistic axions. In [12], a calculation of the Primakoff flux is also given for non-relativistic axions. The derived correction to the flux in the mildly relativistic regime is of the order of 1 % for $m_A = 200$ eV.

2.1.2 Production via ^{57}Fe nuclear magnetic transition

As axions couple to nucleons in many models, another possible mechanism of axion production in the Sun can be their emission following the de-excitation of the low-lying energy levels of some nuclei populated by the high solar temperature. The ability to measure keV-scale energy depositions with EDELWEISS bolometers is an incentive to study more specifically the 14.4 keV monochromatic axions emitted in the M1 transition of ^{57}Fe nuclei.

This particular isotope is considered because of its stability and its remarkable abundance among heavy elements in the Sun (the average ^{57}Fe density in the Sun's core is about $9 \times 10^{19} \text{ cm}^{-3}$ [13]). Last, but not least, its first excited nuclear state, placed at $E^* = 14.4$ keV above the ground state, is low enough to be thermally excited in the hot interior of the Sun, where the average temperature is $kT \sim 1.3$ keV [14, 15]. The conventional relaxation of the excited ^{57}Fe nucleus occurs through the emission of a 14.4 keV photon or an internal-conversion electron. Since this de-excitation corresponds mainly to an M1 transition (E2/M1 mixing ratio is 0.002), also an axion could be emitted.

The effective Lagrangian coupling axions to nucleons is given by:

$$\mathcal{L} = i\bar{\psi}_N \gamma_5 (g_{AN}^0 + g_{AN}^3 \tau_3) \psi_N \phi_A \quad (2.4)$$

where ϕ_A is the axion field, ψ_N is the nucleon isospin doublet, and τ_3 the associated isospin Pauli matrix. The two dimensionless parameters g_{AN}^0 and g_{AN}^3 are the model-dependent isoscalar and isovector axion-nucleon coupling constants, respectively. In KSVZ models they are related to the scale f_A by the following expressions [7, 8]:

$$\begin{aligned} g_{AN}^0 &= -7.8 \times 10^{-8} \left(\frac{6.2 \times 10^6 \text{ GeV}}{f_A} \right) \left(\frac{3F - D + 2S}{3} \right) \\ g_{AN}^3 &= -7.8 \times 10^{-8} \left(\frac{6.2 \times 10^6 \text{ GeV}}{f_A} \right) \left[(D + F) \frac{1-z}{1+z} \right] \end{aligned} \quad (2.5)$$

Here, the dimensionless constants $F = 0.462$ and $D = 0.808$ [16] are invariant matrix elements of the axial current, determined by the hyperon semileptonic decays and flavor $SU(3)$ symmetry. The flavor-singlet axial-vector matrix element S is still a poorly constrained dimensionless parameter. It can be estimated by measurements of the polarized nucleon structure function, but suffers from large uncertainties and ambiguity. Intervals for S proposed in the literature lie in the range $0.15 - 0.55$ [17, 18]. In the model-dependent analysis presented later, we will use the benchmark value $S = 0.5$.

In non-hadronic axions as in the DFSZ model, the values for g_{AN}^0 and for g_{AN}^3 depend on two additional unknown parameters, X_u and X_d [7]. They are related to $\tan \beta_{DFSZ}$, the ratio of two Higgs vacuum expectation values of the model, by the relations $X_u + X_d = 1$ and $X_d = \cos^2 \beta_{DFSZ}$. The expressions for g_{AN}^0 and for g_{AN}^3 are given in this case by [7]:

$$\begin{aligned} g_{AN}^0 &= 5.2 \times 10^{-8} \left(\frac{6.2 \times 10^6 \text{ GeV}}{f_A} \right) \left[\frac{(3F - D)(X_u - X_d - 3)}{6} + \frac{S(X_u + 2X_d - 3)}{3} \right] \\ g_{AN}^3 &= 5.2 \times 10^{-8} \left(\frac{6.2 \times 10^6 \text{ GeV}}{f_A} \right) \frac{D + F}{2} \left(X_u - X_d - 3 \frac{1 - z}{1 + z} \right). \end{aligned} \quad (2.6)$$

In the later model-dependent studies, we will take $\cos^2 \beta_{DFSZ} = 1$ as a benchmark value. Note that this choice also maximises the axio-electric cross section in the DFSZ model, as we will see in Section 2.1.3.

We discuss now in detail the decay of the 14.4 keV first excited state of the ^{57}Fe nucleus to the ground state via axion emission, a process that competes with ordinary M1 and E2 gamma transitions. In general, the axion-to-photon emission rate ratio for the M1 nuclear transition calculated in the long-wavelength limit is [19]:

$$\frac{\Gamma_A}{\Gamma_\gamma} = \left(\frac{k_A}{k_\gamma} \right)^3 \frac{1}{2\pi\alpha} \frac{1}{1 + \delta^2} \left[\frac{g_{AN}^0 \beta + g_{AN}^3}{(\mu_0 - 1/2)\beta + \mu_3 - \eta} \right]^2, \quad (2.7)$$

where k_A and k_γ are the momenta of the outgoing axion and photon respectively, and α is the fine structure constant. The quantities $\mu_0=0.88$ and $\mu_3=4.71$ are the isoscalar and isovector nuclear magnetic moments respectively, given in nuclear magnetons. The parameter δ denotes the E2/M1 mixing ratio for this particular nuclear transition, while β and η are nuclear structure dependent ratios. Their values for the 14.4 keV de-excitation process of an ^{57}Fe nucleus are $\delta=0.002$, $\beta = -1.19$, and $\eta = 0.8$ [15]. Using these values in Eq. (2.7) we find

$$\frac{\Gamma_A}{\Gamma_\gamma} = \left(\frac{k_A}{k_\gamma} \right)^3 1.82 (-1.19g_{AN}^0 + g_{AN}^3)^2. \quad (2.8)$$

Introducing the effective nuclear coupling adapted to the case of ^{57}Fe , $g_{AN}^{\text{eff}} \equiv (-1.19g_{AN}^0 + g_{AN}^3)$, the corresponding axion flux at the Earth, as quoted in [20], is given by:

$$\Phi_{14.4} = \left(\frac{k_A}{k_\gamma} \right)^3 \times 4.56 \times 10^{23} (g_{AN}^{\text{eff}})^2 \text{ cm}^{-2} \text{ s}^{-1}. \quad (2.9)$$

To take into account also non-relativistic limit, the factor $\left(\frac{k_A}{k_\gamma} \right)^3$ has not been set equal to one. Using the expressions given in Eq. (2.5) and Eq. (2.6), it is possible to evaluate g_{AN}^0

and g_{AN}^3 for the DFSZ and KSVZ models and thus evaluate the corresponding fluxes for these two cases. Results show that the two fluxes are of the same order of magnitude (see [21] for a detailed discussion).

2.1.3 Compton, bremsstrahlung and axio-RD processes

The last solar production mechanisms explored in this paper arise if axions couple to electrons. The corresponding effective Lagrangian may be chosen as:

$$\mathcal{L} = ig_{Ae}\bar{\psi}_e\gamma_5\psi_e\phi_A \quad (2.10)$$

where g_{Ae} is the dimensionless axion-electron coupling constant. Axions can then be emitted within the Sun by the Compton process ($\gamma + e^- \rightarrow e^- + A$) and by bremsstrahlung ($e^- + X \rightarrow e^- + X + A$, where X is an electron, a hydrogen or helium nucleus) occurring in the hot plasma. We also consider emission processes associated with the electron capture by an ion (axio-recombination), and to the bound-bound "axio-deexcitation": from the reevaluation by [22], these processes lead to a non-negligible flux, which we call axio-RD. Since the derived fluxes scale in the same way as g_{Ae}^2 , we take into account all these processes at the same time. For the axio-RD process we use a tabulated spectrum from [22] (Fig. 1), while for the Compton-bremsstrahlung process we use the estimation [22]:

$$\begin{aligned} \frac{d\Phi}{dE} &= \left(\frac{d\Phi}{dE}\right)^{\text{Compton}} + \left(\frac{d\Phi}{dE}\right)^{\text{bremsstrahlung}} \\ &= g_{Ae}^2 \times 1.33 \times 10^{33} \text{ E}^{2.987} e^{-0.776 \text{ E}} \\ &\quad + g_{Ae}^2 \times 2.63 \times 10^{35} \text{ E} e^{-0.77 \text{ E}} \frac{1}{1 + 0.667 \text{ E}^{1.278}} \end{aligned} \quad (2.11)$$

where fluxes are in $\text{cm}^{-2} \text{ s}^{-1} \text{ keV}^{-1}$ and energies in keV.

While EDELWEISS data will be used to set model-independent constraints on g_{Ae} , valid for any ALP, explicit expressions for the coupling constant may be given for specific axion models. Within the DFSZ axion models, where the coupling is at the tree level, we have:

$$(g_{Ae})_{\text{DFSZ}} = \frac{m_e}{3f_A} \cos^2 \beta_{\text{DFSZ}} \quad (2.12)$$

where m_e is the electron mass while $\tan \beta_{\text{DFSZ}}$ was already defined in Section 2.1.2. Here again, for model-dependent studies we will fix $\cos \beta_{\text{DFSZ}} = 1$. Therefore, in that case g_{Ae} is numerically given by the expression:

$$(g_{Ae})_{\text{DFSZ}} \simeq 1.68 \times 10^{-4} \frac{\text{GeV}}{f_A} \simeq 2.84 \times 10^{-8} \frac{m_A}{\text{keV}}. \quad (2.13)$$

In the KSVZ axion model characterized by the absence of tree-level coupling to electrons, g_{Ae} is determined only by radiative corrections [8]. As a consequence it is smaller than in the DFSZ model by a factor of about α^2 . The expression for this parameter is:

$$(g_{Ae})_{\text{KSVZ}} = \frac{3\alpha^2 N m_e}{2\pi f_A} \left(\frac{E}{N} \ln \frac{f_A}{m_e} - \frac{2}{3} \frac{4+z+w}{1+z+w} \ln \frac{\Lambda}{m_e} \right), \quad (2.14)$$

where $E/N = 0$ as discussed in Section 2.1.1 for hadronic axions, and $\Lambda \sim 1 \text{ GeV}$ is associated with the QCD confinement scale. We therefore obtain numerically:

$$(g_{Ae})_{\text{KSVZ}} \simeq -5.7 \times 10^{-7} \frac{\text{GeV}}{f_A} \quad (2.15)$$

2.2 Axions as dark matter

Within the cosmological concordance Λ CDM model, a large fraction of the mass content of the universe is composed of dark matter (DM), the nature of which is still unknown. In particular the dynamics of our galaxy can be explained by the presence of a non-relativistic dark matter halo with a solar neighborhood density $\rho_{\text{DM}} = 0.3 \text{ GeV}/\text{cm}^3$ in the conventional model. Axion-like particles are a possible candidate for dark matter, and the hypothesis of keV-scale ALPs was in particular proposed as an explanation of the annual modulation observed by DAMA in NaI crystals [23].

When testing this scenario, we will assume that axions constitute all of the galactic dark matter. The total, average flux of dark matter axions on Earth is then:

$$\Phi_{\text{DM}} [/\text{cm}^2/\text{s}] = \rho_{\text{DM}} \cdot v_A / m_A = 9.0 \times 10^{15} \left(\frac{\text{keV}}{m_A} \right) \cdot \beta \quad (2.16)$$

In this expression, m_A is the axion mass and v_A the mean axion velocity distribution with respect to the Earth, $\beta \simeq 10^{-3}$. The flux does not depend on any axion coupling.

3 Axion interactions in EDELWEISS detectors

In this paper we will use, depending on the production channel, two different mechanisms for axion detection.

- Through the Primakoff effect, axions can be converted into photons in the intense electric field of the germanium crystal [24]. The wavelength of relativistic solar axions, with an energy of a few keV, is of the same order of magnitude as the inter-atomic spacing of the detector. Therefore, depending on the direction of the incoming axion flux with respect to the lattice, the axion signal can be enhanced significantly through Bragg diffraction (EDELWEISS detectors are mono-crystals). The corresponding correlation of the count rate with the position of the Sun in the sky also helps further with an effective background rejection. We can express the Bragg condition as a function of the axion energy, neglecting the axion mass and the target recoil: $E_A = |\mathbf{G}^2| / (2\mathbf{u} \cdot \mathbf{G})$, where \mathbf{G} is a reciprocal lattice vector and \mathbf{u} is a unit vector directed towards the Sun. For non-zero axion masses, the Bragg condition is changed by the axion dispersion relation and becomes, for $m_A \ll E_A$:

$$E_A^2 = \frac{\mathbf{G}^4}{4(\mathbf{u} \cdot \mathbf{G})^2} + \frac{m_A^2}{2} \quad (3.1)$$

For $m_A = 200 \text{ eV}$, the relative correction on E_A with respect to the case of massless axions is $m_A^2/4E_A^2 \sim 10^{-2} E_A$.

- Axions can also be detected through the axio-electric effect, the equivalent of a photo-electric effect with the absorption of an axion instead of a photon: $A + e^- + Z \rightarrow e^- + Z$. The axio-electric cross-section as a function of the axion energy was computed in [21, 25, 26], and is represented for several values of its mass in Fig. 2:

$$\sigma_{Ae}(E) = \sigma_{\text{pe}}(E) \frac{g_{Ae}^2}{\beta} \frac{3E^2}{16\pi\alpha m_e^2} \left(1 - \frac{\beta^{\frac{2}{3}}}{3}\right) \quad (3.2)$$

In this expression σ_{pe} is the germanium photoelectric cross-section, taken from [27], β is the ratio of the axion velocity to the speed of light, α is the fine structure constant and m_e the electron mass. Through the axio-electric effect, an incoming axion of energy E (relativistic or not) will generate an electron recoil with the same energy within an EDELWEISS detector.

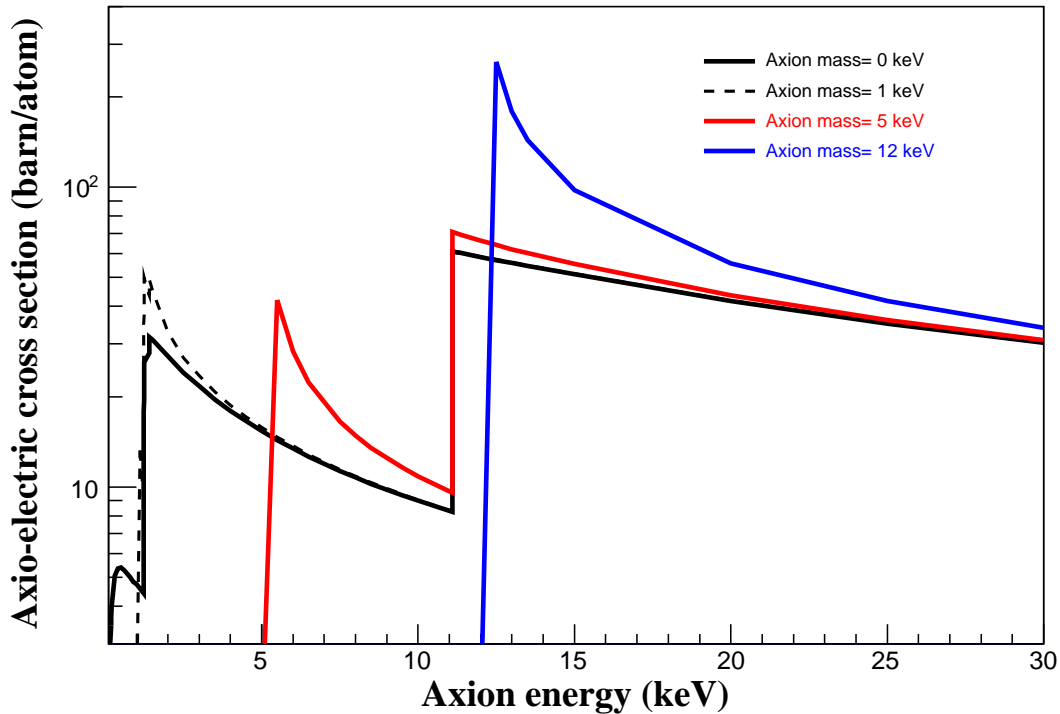


Figure 2. Axio-electric cross section for different axion masses, computed for germanium and normalized with $g_{Ae} = 1$. The discontinuities at 1.2 – 1.4 keV and 11.1 keV are due to electron shell energies.

4 EDELWEISS-II data and backgrounds

EDELWEISS was primarily designed as a direct detection WIMP (Weakly Interacting Massive Particle) search experiment, in which nuclear recoils induced by WIMPs from the galactic halo are detected using germanium detectors working at very low temperatures (18 mK). We simultaneously measure ionization and phonon signals. The comparison of the two signals allows a separation on an event-by-event basis of nuclear recoils from electron recoils induced by β and γ radioactivity. These electron recoils constitute the major source of background in most present-day direct WIMP searches. In particular, the ten 400-g EDELWEISS-II detectors

used in this analysis, called InterDigit (ID), are equipped with a set of thin aluminium interleaved electrodes. This makes possible the identification of near-surface interactions based on the measured ionization signals [10], and therefore the definition of an inner, so-called fiducial volume for each detector. Detectors are operated at the Underground Laboratory of Modane (LSM) in the Frejus Tunnel under the French-Italian Alps. They are protected from external radioactivity by lead and polyethylene shields and also an active muon veto. EDELWEISS-II has provided frontier sensitivities to WIMP-nucleon cross-sections for WIMP masses above 50 GeV [28, 29], as well as for low-mass WIMPs ~ 10 GeV [30].

Through their weak coupling either to photons or to electrons, axions generate electron recoils which can be detected in the EDELWEISS bolometers. The axion searches presented here are based on data collected with ten ID bolometers during 14 months in 2009-2010, as described in [28, 29]. The offline pulse reconstruction and calibration are identical to [28, 29]. Axion-induced events were searched for within the population of low-energy fiducial, electronic recoils:

- Fiducial events were selected by requiring the absence of any signal above 4 sigma on the veto and guard electrodes and by constraining the difference in the measured values of the two collecting electrodes. The efficiency of this cut results in a fiducial mass of 160 g for each detector [28].
- For each fiducial event, we measured both the heat energy E_{heat} and a fiducial ionization energy E_{ion} , based on the combination of signals from both collecting electrodes. Fiducial electron recoils are gaussian distributed along the line $E_{\text{ion}} = E_{\text{heat}}$. We rejected events beyond three standard deviations from this line.

An exposure adapted to this event selection was defined: we discarded time periods with noisy fiducial ionization or heat signals, and obtained a homogeneous data set for each detector with 280 live days on average. The total exposure reaches 448 kg.d for this analysis. It is larger than the WIMP-search exposure published in [29] mainly because the axion search does not depend as strongly on the purity of the fiducial selection, and requirements on the resolution on the heat and ionization guard signals can be relaxed. To reject misreconstructed pulses, a cut was applied on the χ^2 of the fit to heat pulse shapes, keeping 98.7 % efficiency. We also rejected coincidence events in neighboring bolometers and events detected in the muon veto. The latter has negligible deadtime [31].

At low energies, an efficiency loss ϵ_{online} appears because of the online trigger. The efficiency function was computed from our knowledge of the time variations of this trigger. It was cross-checked with gamma calibrations. In addition, we selected events with both heat and fiducial ionization above a given threshold defined on a per-detector basis. The cut on fiducial ionization is essential to remove the large number of heat-only pulses recorded during the experiment. They are due to lead recoils associated with surface radioactivity, internal radioactivity of the heat sensors and mechanical noise.

Finally, for each selected event we combined the heat and fiducial ionization to obtain an optimal energy estimator for fiducial electron recoils: $\tilde{E} = w_{\text{heat}} E_{\text{heat}} + w_{\text{ion}} E_{\text{ion}}$ where w_{heat} and w_{ion} are weights depending on the heat and fiducial ionization resolutions. An analysis threshold on \tilde{E} is set for each detector, by requiring that $\epsilon_{\text{online}}(\tilde{E}) > 50\%$ and $\epsilon_{\text{other cuts}}(\tilde{E}) > 95\%$. With these cuts, three detectors have a threshold at 2.5 keV, two at 3 keV and five at 3.5 keV. The average FWHM at low energy is 0.8 keV for \tilde{E} .

Fig. 3 (left) shows the event rate as a function of \tilde{E} for a typical detector, after the data selection described above and after correction by the online trigger efficiency function.

The background consists of a Compton profile with a smooth, slightly decreasing energy dependence, together with radioactive peaks, notably identified at 10.37 keV (^{68}Ge), 9.66 keV (^{68}Ga), 8.98 keV (^{65}Zn), 6.54 keV (^{55}Fe), 5.99 keV (^{54}Mn) and 4.97 keV (^{49}V). An additional smooth background increase at low energy may also be expected from unrejected surface interactions. In the axion searches described below, two different background models are used depending on the search:

1. *Primakoff solar axions.* In this study, we will exploit the time and energy dependence of the axion signal to quantify $g_{A\gamma}$. This results in an effective background rejection of about two orders of magnitude [32]. Furthermore the expected global energy distribution of the signal has a larger width than the detector FWHM. As a consequence we will include all radioactive peaks in the background model used for this analysis, in addition to a smooth component. The smooth time variation of these peaks is negligible with respect to the sharp and fast-varying axion signal. This analysis also requires that we first study each detector individually: a background model is adjusted to each detector spectrum.
2. *Other axion searches.* In all other searches, the axion signal has no time dependence to first order and is simply identified by its spectral shape (such as a line) in the stacked spectrum of all detectors. The time evolution of the 8.98 keV and 10.37 keV line intensities (with decay times of 243 and 271 days, respectively) allowed us to measure the intensity of these specific cosmogenic lines and include them in the background model, independently from a potential time-independent axion signal at the same energy. However, the other radioactive peaks cannot be confidently estimated from their decrease with time for lack of statistics. Therefore they are conservatively not included in the background model. Above 12 keV, the smooth component of the spectrum is adjusted by a polynomial fit. In this energy region, an increase of the count rate is observed when energy decreases as expected from simulations [33]. The smooth component is extrapolated below 12 keV with a linear fit. Two detectors, having a significantly higher background than the others below 8 keV [30], were discarded from the stacked spectrum below this energy. This results in an effective exposure of 357 kg.d at low energy for these analyses. Fig. 3 (right) shows the stacked, efficiency-corrected background rate of the detectors used in the analysis, together with the associated background model. We will refer to this model as $B(\tilde{E})$ in the following.

5 Axion search: Primakoff solar axions

We consider the scenario in which axions are produced in the Sun by inverse Primakoff conversion, resulting in the flux given in Eq. (2.3), and are detected again by the Primakoff effect, using coherent Bragg diffraction. This axion search relies only on the existence of an effective axion-photon coupling. Using the same formalism as in [32], the expected count rate in a single detector as a function of energy, time, and the detector orientation α is given by:

$$\begin{aligned}
 R(\tilde{E}, t, \alpha) &= 2(2\pi)^3 \frac{V}{v_a^2} \sum_{\mathbf{G}} \frac{d\phi}{dE_A} \frac{g_{A\gamma}^2}{16\pi^2} \sin^2(2\theta)^2 \frac{1}{|\mathbf{G}|^2} |S(\mathbf{G})F_A^0(\mathbf{G})|^2 W(E_A, \tilde{E}) \\
 &= \left(\frac{g_{A\gamma} \times 10^8}{\text{GeV}^{-1}} \right)^4 \bar{R}(\tilde{E}, t, \alpha) \equiv \lambda \bar{R}(\tilde{E}, t, \alpha).
 \end{aligned}
 \tag{5.1}$$

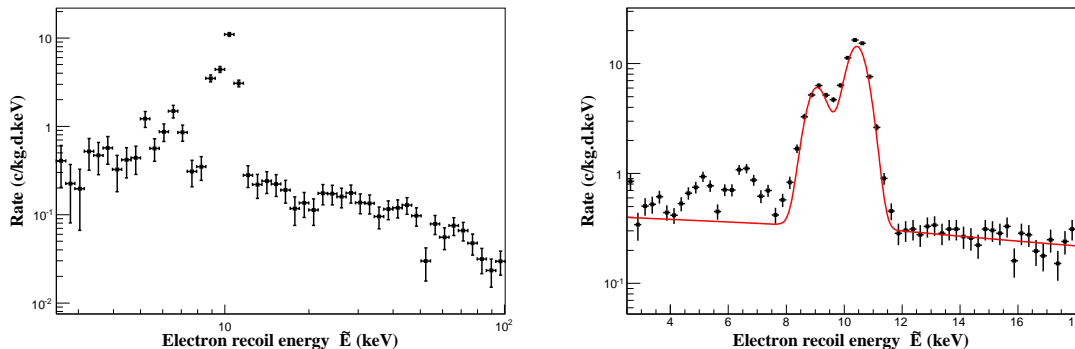


Figure 3. Left: Efficiency-corrected electron recoil spectrum in the fiducial volume of a single bolometer called ID3, in the energy range 2.5 – 100 keV. The smooth Compton feature is visible as well as low-energy lines from induced radioactivity and cosmogenic activation of germanium. Right: Stacked, efficiency-corrected electron recoil spectrum for the full exposure in the 2.5 – 18 keV range. The red line is the background model $B(\tilde{E})$ used in all analyses but Primakoff: a smooth Compton component linearly extrapolated below 12 keV, together with 10.37 keV and 8.98 keV cosmogenic lines.

In the first expression, V is the detector volume and v_a is the volume of the elementary cell of the crystal lattice. The sum is over the vectors \mathbf{G} of the reciprocal lattice, 2θ is the scattering angle (related to the time-varying direction of the Sun with respect to \mathbf{G}), S is the structure factor and F_A^0 is the atomic form factor associated with the electrostatic field. The function W represents the detector resolution for the observable energy \tilde{E} , E_A is the axion energy related to \mathbf{G} by the Bragg condition. Fig. 4 illustrates both time and energy variation of the signal, for a given detector orientation in local (terrestrial) coordinates. Note that this expression for the rate still applies for mildly relativistic axions, after the appropriate modifications of both the Bragg condition giving E_A and the solar flux are taken into account. Up to $m_A \simeq 200$ eV, the solar Primakoff flux changes by less than 1 % and the Bragg energy is shifted by ~ 1 %, a negligible value with respect to detector resolution hence the expression remains valid.

The geodesic location of the Underground Laboratory of Modane is (45.14° N, 6.68° E). While the vertical axis of the bolometer tower is aligned with the [001] axis of each detector, with a precision of about one degree, the individual azimuthal orientation α of each detector was not measured. Therefore, in a first step we will adapt the method developed in the same context by [32] for a single bolometer. We use the following time correlation function assuming a given orientation α :

$$\chi_k(\alpha) = \epsilon_k \sum_i [\overline{R_k}(t_i) - \langle \overline{R_k} \rangle] \cdot n_{ik} \equiv \sum_i^n W_{ik} \cdot n_{ik} \quad (5.2)$$

where ϵ_k is the detector efficiency, n_i indicates the number of measured events in the time interval $[t_i, t_i + \Delta t]$, the index k refers to the energy interval $[\tilde{E}_k, \tilde{E}_k + \Delta \tilde{E}]$ and the sum is over the total period of data taking. We use the analysis window 3 – 8 keV, which contains most of the expected signal. The Dirac-like brackets indicate an average over time. The distribution of n_i is given by a Poisson distribution with average:

$$\langle n_{ik} \rangle = \epsilon_k [\lambda \overline{R_k}(t_i) + b_k] \Delta t \Delta \tilde{E} \quad (5.3)$$

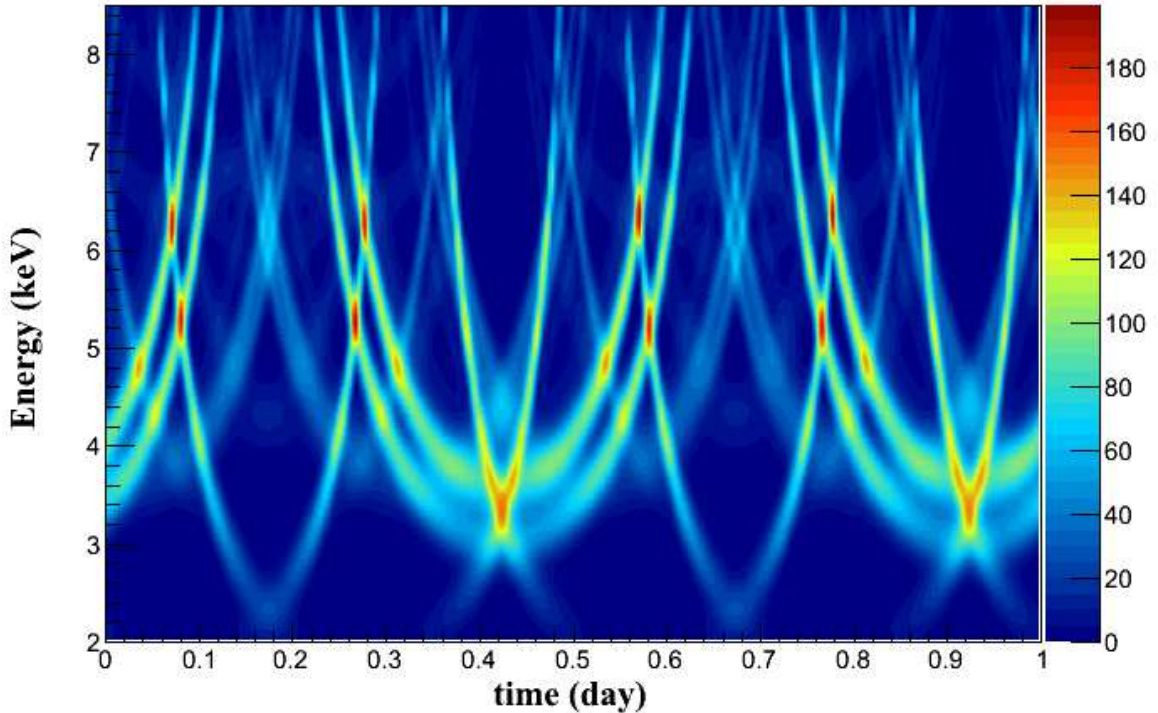


Figure 4. Example of the theoretical Primakoff conversion signal in a single detector, in counts per kg.d.keV, for a detector resolution of 0.5 keV and $g_{A\gamma} = 10^{-8} \text{ GeV}^{-1}$.

where b_k is the individual, constant detector background in the considered energy interval. Assuming background dominates, we compute¹:

$$\begin{aligned} \langle \chi_k \rangle &= \epsilon_k^2 \lambda \sum_i W_{ik}^2 \Delta t \Delta \tilde{E} \equiv \lambda \cdot A_k \\ \sigma^2(\chi_k) &\approx \epsilon_k b_k A_k \end{aligned} \quad (5.4)$$

Minimizing the associated likelihood function, we derive a simple estimator for the reduced coupling λ :

$$\tilde{\lambda}(\alpha) = \frac{\sum_k \frac{\chi_k}{\epsilon_k b_k}}{\sum_k \frac{A_k}{\epsilon_k b_k}} \quad (5.5)$$

In order to combine all the detectors and at the same time take into account the lack of knowledge of the azimuthal orientation of each crystal, we apply the following procedure. Combining all detectors and scanning over all possible orientations, we obtain from the data an overall distribution for $\tilde{\lambda}$, $D_{\text{real data}}(\tilde{\lambda})$. We performed Monte Carlo simulations including the detector exposures, efficiencies and backgrounds as well as a potential axion signal. These simulations show that, in the presence of an axion signal, this distribution D charts a tail at high $\tilde{\lambda}$. Based on simulations, we therefore introduce a statistical observable I given by:

¹This corrects the expression found in [32].

$$I = \int_{|\tilde{\lambda}| < \tilde{\lambda}_c} D(\tilde{\lambda}) - \int_{|\tilde{\lambda}| > \tilde{\lambda}_c} D(\tilde{\lambda})$$

where $\tilde{\lambda}_{\text{cutoff}} = 0.003$. The simulations allow us to obtain the expected distribution of I for a given λ_0 and set of detector orientations² α_0^{bolo} . The measured value $I_{\text{real data}}$ is compatible with simulations carried out for $\lambda_0 = 0$. By scanning over λ_0 and comparing the resulting distributions of I with $I_{\text{real data}}$, we can place a 95% CL upper limit on the axion-photon coupling:

$$g_{A\gamma} < 2.13 \times 10^{-9} \text{ GeV}^{-1} \quad (95\% \text{CL}).$$

This limit is shown in Fig. 5 and compared with constraints from other experiments and astrophysical bounds. These results will be discussed in more details in Section 9.

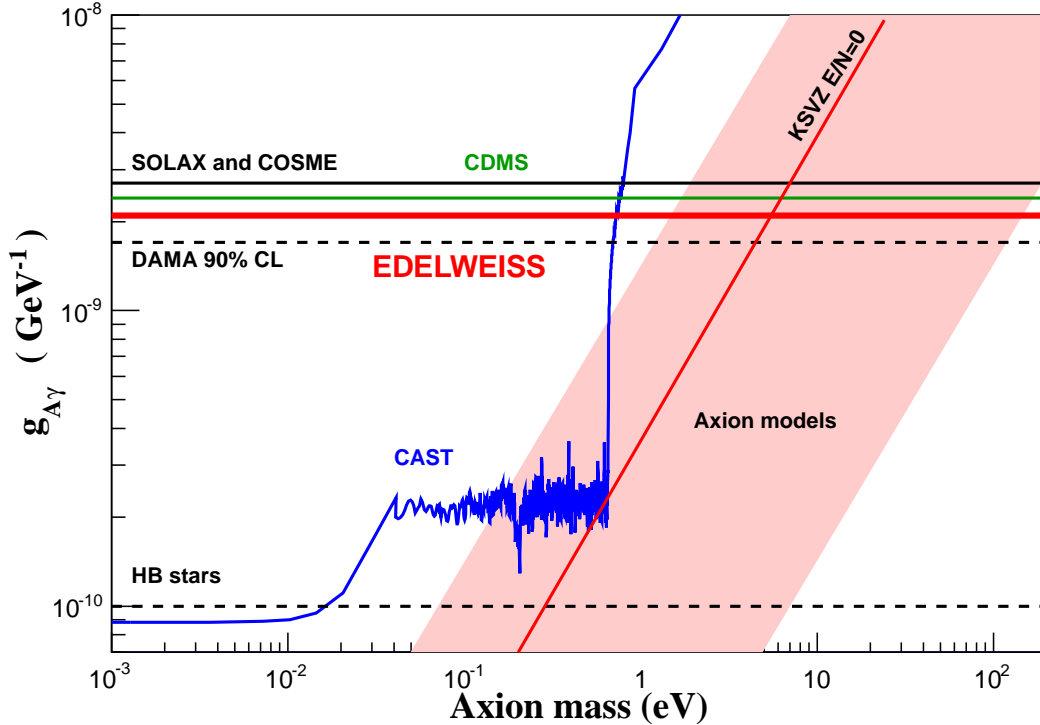


Figure 5. 95 % CL limit on the $g_{A\gamma}$ coupling from the solar Primakoff flux obtained by EDELWEISS-II (red), compared to other crystal experiments such as SOLAX [34], COSME [35], CDMS [36] (green) and DAMA [37] (90 % CL)). We also show the CAST limit [38] (blue) and indirect bounds from HB stars [39]. The light red band labeled ‘Axion models’ represents typical theoretical models with $|E/N - 1.95| = 0.07-7$. The red solid line inside this band represents the case $E/N=0$ (KSVZ model).

6 Axion search: 14.4 keV solar axions

We now test the scenario in which solar axions are produced in the ^{57}Fe magnetic transition and detected by the axio-electric effect in a Ge crystal, resulting in a 14.4 keV electron recoil.

²Note that this procedure is independent of the chosen orientation of the detectors.

The expected rate in counts per keV is the product of the flux $\Phi_{14.4}$ (Eq. 2.9), $\beta = v/c$, the axio-electric cross section given in Eq. (3.2), the individual detector resolution σ_i and exposure $M_i T_i$, summing over all detectors i :

$$R_{14.4}(\tilde{E}) = \beta^3 \Phi_{14.4} \sigma_A(14.4) \sum_i M_i T_i \frac{1}{\sqrt{2\pi}\sigma_i} \times e^{-\frac{(\tilde{E}-14.4)^2}{2\sigma_i^2}} \quad (6.1)$$

$$\equiv \lambda \times \overline{R}_{14.4}(\tilde{E}) \quad \text{where } \lambda = (g_{Ae} \times g_{AN}^{\text{eff}})^2$$

At 14.4 keV, the online trigger efficiency is equal to 1 for all 10 detectors. Fig. 6 shows the stacked electron recoil spectrum in the 12 – 18 keV interval. There is no hint of a line at 14.4 keV and we therefore derive a limit on the line intensity using a binned likelihood function and assuming Poisson statistics for the background:

$$L = \prod_i e^{-N_i^{\text{th}}} \frac{(N_i^{\text{th}})^{N_i^{\text{exp}}}}{N_i^{\text{exp}}!} \quad (6.2)$$

Here N_i^{exp} is the observed number of events in the energy bin i and $N^{\text{th}}(\tilde{E}) = \lambda \overline{R}_{14.4}(\tilde{E}) + B(\tilde{E})$.

The likelihood function is gaussian to a very good approximation. In order to deal with possible negative background fluctuations, we use the following prescription. If the likelihood best fit is positive we use a standard gaussian 90% upper limit, the value is negative we assume it is equivalent to a zero measurement. This is a conservative approach which solves issues of undercoverage and empty intervals as discussed in [40]. We find $R_{14.4} < 0.038$ counts/kg/d. This method was validated with MC simulations.

For a low-mass axion, this result translates to a 90% CL constraint on the couplings:

$$g_{AN}^{\text{eff}} \times g_{Ae} < 4.7 \times 10^{-17}$$

Using the relationships given in Eq.(2.9) and Eq.(3.2), it is possible to obtain the upper limits for $g_{AN}^{\text{eff}} \times g_{Ae}$ as a function of the axion mass m_A for axion masses up to 14 keV. Fig. 7 shows this model independent limit.

7 Axion search: Compton, bremsstrahlung and axio-RD

In this scenario, solar axions are produced through Compton, bremsstrahlung and axio-RD processes, resulting in the flux given by Eq. (2.11). These axions can be detected by the axio-electric effect in the crystal, resulting in an expected count rate given by:

$$R_{\text{C-B-RD}}(\tilde{E}) = \int dE_A \sigma_A(E_A) \left(\frac{d\Phi^{\text{C-B-RD}}}{dE_A} \right) \times \sum_i \epsilon_i(\tilde{E}) M_i T_i \frac{1}{\sqrt{2\pi}\sigma_i} \times e^{-\frac{(\tilde{E}-E_A)^2}{2\sigma_i^2}} \quad (7.1)$$

$$\equiv \lambda \times \overline{R}_{\text{C-B-RD}}(\tilde{E}) \quad \text{where } \lambda = g_{Ae}^4$$

The notations are identical to Eq. (6.1), ϵ_i being the efficiency function for a given detector i , which is relevant at low energy. We look for Compton-bremsstrahlung-axio-RD solar axions in the 2.5 – 30 keV energy window, which contains most of the signal (see Fig. 1). We use the same likelihood procedure described in the previous section, where $N^{\text{th}}(\tilde{E})$ becomes:

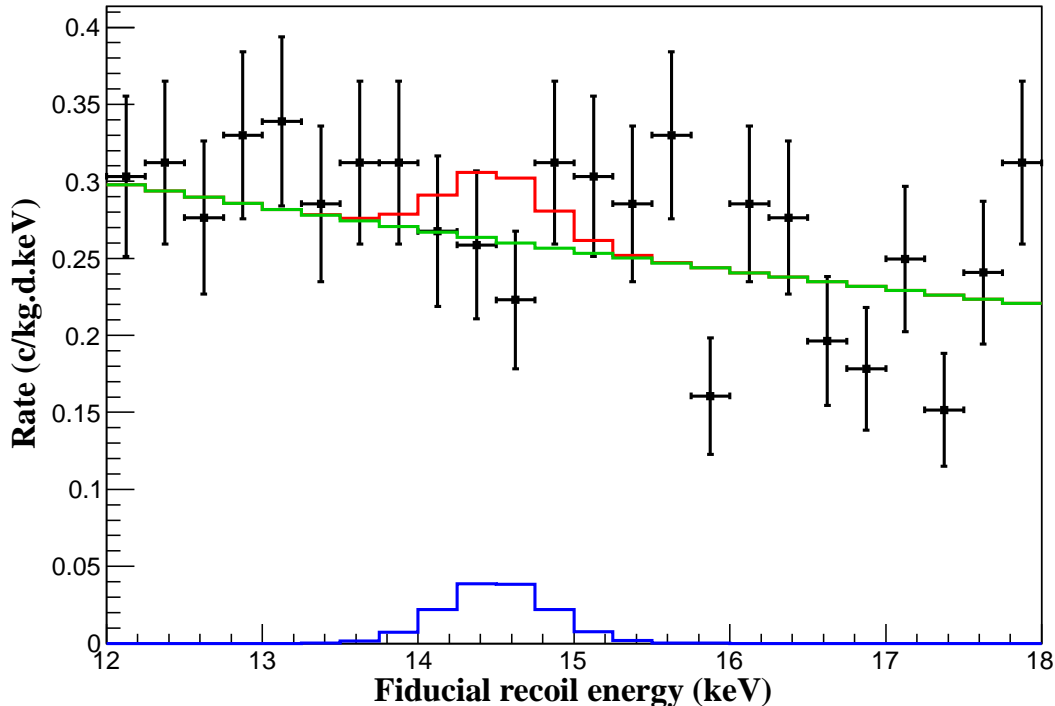


Figure 6. Stacked electron recoil spectrum around 14.4 keV. Blue: detector response to 14.4 keV solar axions using axio-electric conversion at the 90% CL limit. Green: background model. Red: axion signal with coupling at the 90% CL limit superimposed on the background model.

$$N^{th}(\tilde{E}) = \lambda \bar{R}_{C-B-RD}(\tilde{E}) + B(\tilde{E}) \quad (\lambda = g_{Ae}^4) \quad (7.2)$$

The expected signal is not a line feature, so the likelihood analysis window has been tailored to each axion mass. Fig. 8 shows an example for $m_A = 0$ keV, for which the expected signal stands mostly below 5 keV, and therefore the likelihood is not strongly affected by the presence of activation peaks. For $m_A > 5$ keV, the presence of the peaks, not included in the background model $B(\tilde{E})$, degrades the sensitivity to axions. For each axion mass, a 90 % CL limit is found using the same prescription as before. The constraint found for axions with $m_A \ll$ few keV is $R_{C-B-RD} < 0.46$ counts/kg/day. This translates to a constraint on the axio-electric coupling: $g_{Ae} < 2.56 \times 10^{-11}$ at 90% CL. The evolution of the limit on g_{Ae} as a function of m_A can be found on Fig. 11.

8 Axion search: dark matter axions

We now focus on the scenario in which axions constitute the entire dark matter halo of our galaxy. Since the galactic DM is non-relativistic, the resulting signal due to the axio-electric coupling will consist in electron recoils at an energy equal to the axion mass m_A . From Eq. (2.16) and Eq. (3.2), the expected axion count rate is:

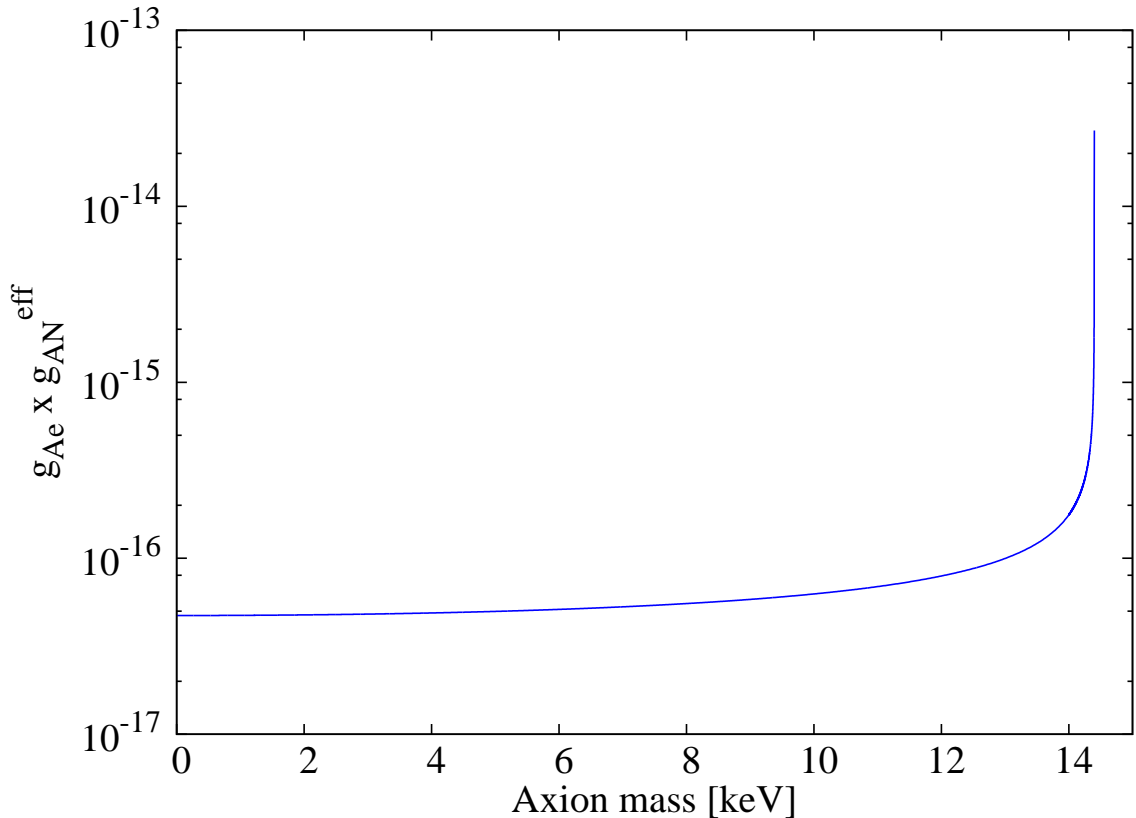


Figure 7. 90 % CL upper limits for $g_{Ae} \times g_{AN}^{\text{eff}}$ as a function of the axion mass m_A obtained with the EDELWEISS-II data.

$$\begin{aligned}
 R_{\text{DM}}(\tilde{E}) &= \Phi_{\text{DM}} \sigma_A(m_A) \times \sum_i \epsilon_i(\tilde{E}) M_i T_i \frac{1}{\sqrt{2\pi}\sigma_i} \times e^{-\frac{(\tilde{E}-m_A)^2}{2\sigma_i^2}} \\
 &= \lambda \times \bar{R}_{\text{DM}}(\tilde{E}) \quad \text{where } \lambda = g_{Ae}^2
 \end{aligned}
 \tag{8.1}$$

The notations are the same as above. We look for galactic axions in the [2.5 keV - 100 keV] mass window. We proceed with a binned likelihood as in Eq. (6.2), where

$$N^{th}(\tilde{E}) = \lambda \bar{R}_{\text{DM}}(\tilde{E}) + B(\tilde{E})
 \tag{8.2}$$

Over the whole energy range, no statistically significant excess was found, except at energies where potential cosmogenic lines are expected. We therefore report a 90% CL limit on the axion coupling as a function of its mass. We use the same prescription as above to derive the appropriate limit. The shape of our electron recoil background implies that the strongest constraint is found for 12- keV axions, for which we found $R_{\text{DM}} < 0.05$ counts/kg/d. This translates to a constraint on the dark matter axio-electric coupling at this mass: $g_{ae} < 1.05 \times 10^{-12}$. The limit on g_{Ae} within this scenario is represented as a function of m_A in Fig. 9.

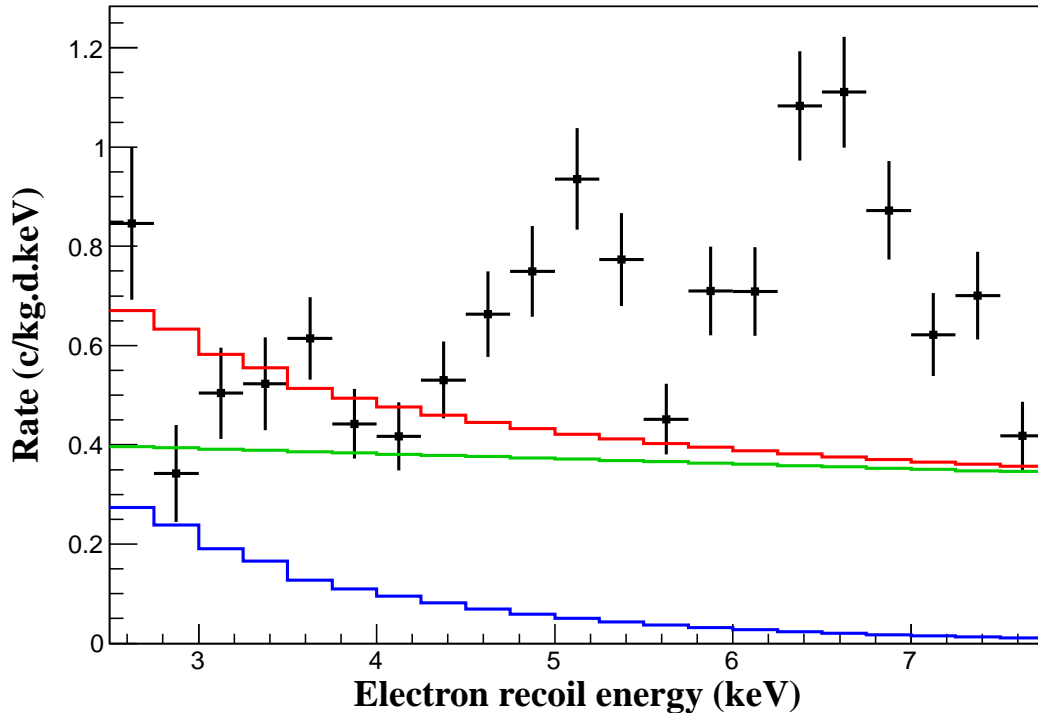


Figure 8. Efficiency-corrected stacked electron recoil spectrum for the whole exposure, close to the analysis threshold. The detector response for a Compton Bremsstrahlung axio-RD, zero-mass axion signal at the 90% confidence limit is represented by the blue curve, while the green curve shows the conservative background model. Red curve: signal superimposed over the background model. Note that the number of detectors used to compute the spectrum depends on the energy range considered.

9 Results and discussion

Channel	14.4 ($g_{Ae} \times g_{AN}^{\text{eff}}$)	DM (g_{Ae})	C-B-RD (g_{Ae})	P ($g_{A\gamma}$)
Limit	$< 4.70 \times 10^{-17}$	$< 1.05 \times 10^{-12}$	$< 2.56 \times 10^{-11}$	$< 2.13 \times 10^{-9} \text{ GeV}^{-1}$

Table 1. Summary of the limits on the different axion couplings. 14.4 stands for 14.4 keV solar axions, DM for dark matter axions, C-B-RD for Compton-bremsstrahlung and axio-RD axions, and P for Primakoff axions. The quoted values are in the limit $m_A = 0$, except for the dark matter case, which is given for $m_A = 12.5$ keV. All limits are at 90% CL except P (95% CL).

Using the Sun as a potential source for axions, or under the hypothesis that galactic dark matter is made of axions, we set model-independent constraints on the couplings of ALPs or axions to gamma-rays, electrons, and nucleons. Table 1 summarizes the limits obtained for each channel on the respective couplings:

- The Primakoff axion search is characterized by a specific time and spectral dependence of the signal. The combination of low effective background and large exposure results in a 95 % CL limit of $g_{A\gamma} < 2.13 \times 10^{-9} \text{ GeV}^{-1}$, an improvement with respect to other

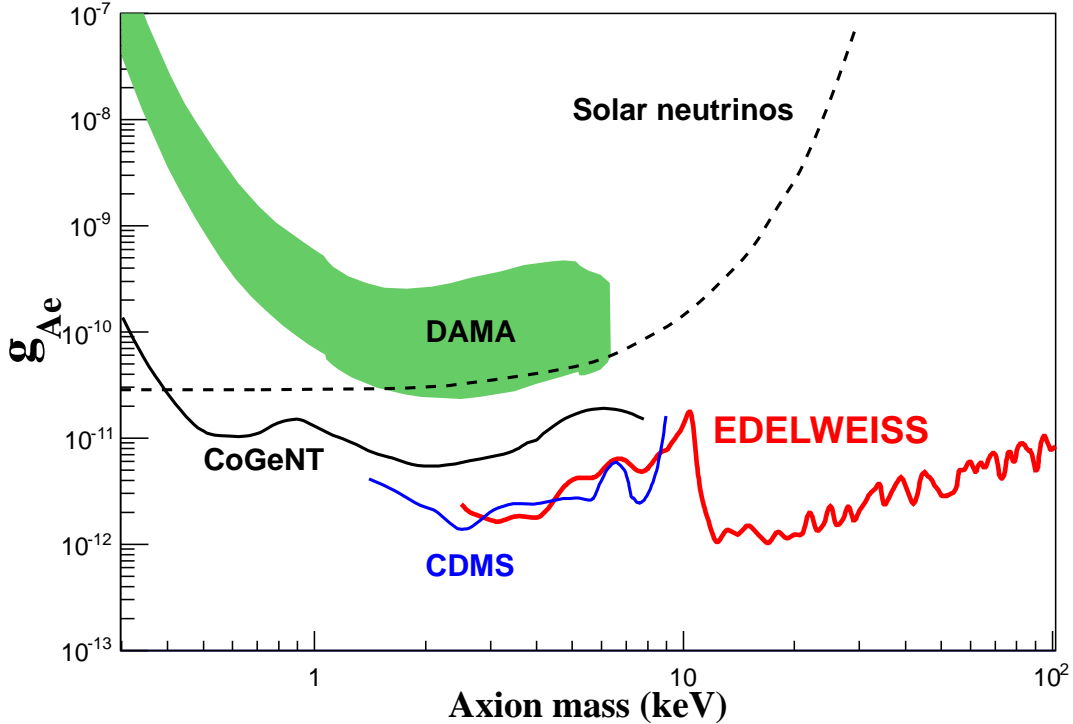


Figure 9. Limit on the axion-electron coupling as a function of m_A assuming the local dark matter halo of our galaxy is made entirely of axions. The green contour corresponds to a possible interpretation of the DAMA annual modulation signal [23], while the black and blue curves are constraints set by the CoGeNT [41] and CDMS [36] germanium detectors respectively. Dashed line: indirect bound derived from the solar neutrino flux measurement [42].

germanium crystal-based searches [34–37]. Especially for $\sim 1 - 100$ eV axions, the only other non-crystal constraints are indirect constraints derived from stellar physics.

- In a search for solar axions produced by Compton-bremsstrahlung and axio-RD processes, we provide a model-independent limit on g_{Ae} which is currently the best direct constraint on this coupling compared to [43, 44]. This limit also slightly improves the indirect bound obtained from the solar neutrino flux measurement [42].
- The search for solar axions emitted by ^{57}Fe provides first a model-independent limit on $g_{Ae} \times g_{AN}^{\text{eff}}$, which improves the one presented in [21]. It is possible, as a second approach, to calculate the allowed range of g_{Ae} as a function of the axion mass m_A , using values predicted by the DFSZ and KSVZ models for the couplings g_{AN}^0 and g_{AN}^3 . The resulting constraints are shown in Figure 10.
- We also tested the specific scenario in which the galactic dark matter halo is made of ALPs with a keV-scale mass. We found a limit similar to the one of CDMS [36] that we extended up to 100 keV. The limit, as CDMS and CoGeNT [41], constrains such an interpretation of the observed DAMA feature [23].

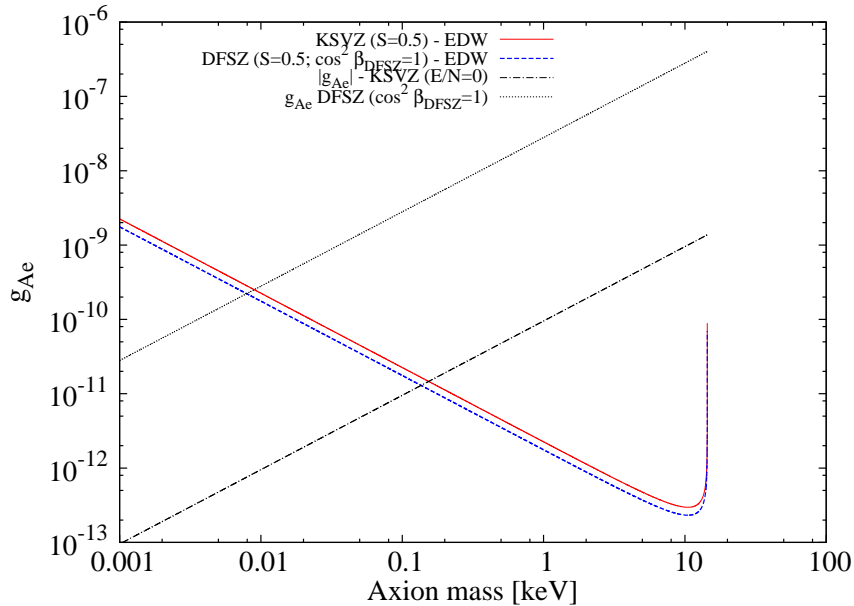


Figure 10. Limits on g_{Ae} assuming values predicted by the DFSZ and KSVZ models for the couplings g_{AN}^0 and g_{AN}^3 . The curves are calculated with the assumption $S = 0.5$ for the flavor-singlet axial vector matrix element in both models and $\cos^2 \beta_{\text{DFSZ}} = 1$ for the DFSZ model.

Fig. 11 presents a summary of all limits on g_{Ae} , some of which are valid only within a given scenario.

Channel	14.4 ($g_{Ae} \times g_{AN}^{\text{eff}}$)	C-B-RD (g_{Ae})	P ($g_{A\gamma}$)
KSVZ	$154 \text{ eV} < m_A < 14.4 \text{ keV}$	$269 \text{ eV} < m_A < 40 \text{ keV}$	$5.73 < m_A \lesssim 200 \text{ eV}$
DFSZ	$7.93 \text{ eV} < m_A < 14.4 \text{ keV}$	$0.91 \text{ eV} < m_A < 80 \text{ keV}$	$14.86 < m_A \lesssim 200 \text{ eV}$

Table 2. Excluded ranges of axion masses derived from EDELWEISS-II constraints within two benchmark models, KSVZ and DFSZ. We assume axion and hadronic parameters described in Section 2. The channels considered are solar 14.4 keV axions (14.4), solar Compton-bremsstrahlung-RD axions (C-B-RD) and solar Primakoff axions (P).

Within the framework of a given axion model, KSVZ or DFSZ, the only free parameter is the axion mass, or equivalently the Peccei-Quinn symmetry-breaking scale f_A (see Eq. (1.1)). Therefore, our limits on the couplings constrain m_A directly. We calculate the exclusion range for m_A from each of the three solar axion channels previously studied, within both models assuming the model-dependent couplings and hadronic physics parameters given in Section 2. Note that we do not use the dark matter channel here since keV-scale KSVZ or DFSZ axions cannot constitute the local dark matter halo as they are not cold dark matter. In addition, we observe that the limit related to the constraint on $g_{A\gamma}$ holds for mildly relativistic solar axions, up to $m_A \lesssim 200 \text{ eV}$. In Table 2, the derived limits on the axion mass are summarized for both benchmark models. Within the DFSZ model we completely exclude the mass range $0.91 \text{ eV} < m_A < 80 \text{ keV}$ from the Compton-bremsstrahlung-RD channel only. Other channels are complementary in specific subintervals. Within the KSVZ framework, combining the 14.4 keV and Compton-bremsstrahlung-RD channels, we exclude the mass range $154 \text{ eV} < m_A < 40 \text{ keV}$. The Primakoff channel also excludes relativistic solar axions

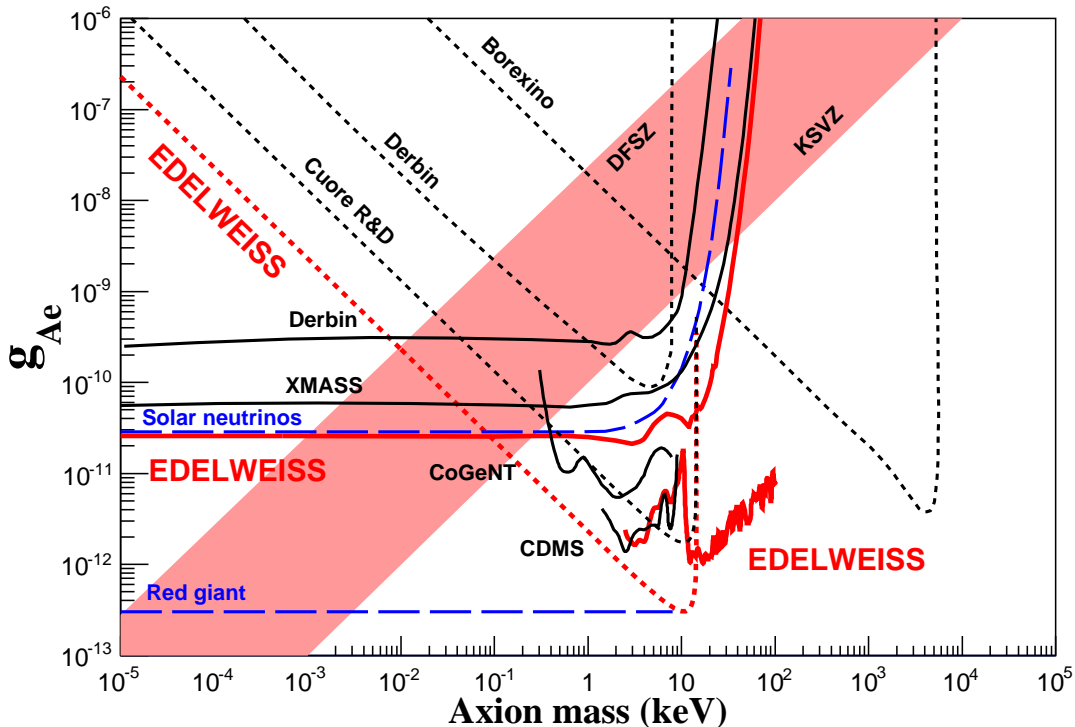


Figure 11. Summary of the constraints obtained by EDELWEISS-II on the g_{Ae} axion coupling as a function of m_A . The EDELWEISS limits are in red. Continuous lines starting at $m_A = 0$, including Derbin [43] and XMASS [44]: model-independent limit on g_{Ae} from the solar Compton-bremsstrahlung-recombination flux. Continuous lines in the keV mass range, including CoGeNT [41] and CDMS [36]: limits on the coupling of axions assuming they constitute all local galactic dark matter. Dotted lines, including CUORE R&D [21], Derbin [45] and Borexino [46]: bounds on g_{Ae} , derived from constraints on $g_{Ae} \times g_{AN}^{\text{eff}}$ on various nucleus by assuming that g_{AN}^{eff} follows the DFSZ model with $\cos \beta_{\text{DFSZ}} = 1$. Benchmark DFSZ and KSVZ models are represented by a shaded band. Indirect astrophysical bounds from solar neutrinos [42] and red giants [47] are represented in dashed lines.

with $m_A > 5.73$ eV, therefore closing the window for $5.73 \text{ eV} < m_A < 40$ keV axion masses.

10 Conclusions

We have used data from the EDELWEISS-II detectors, originally used for WIMP searches, to constrain the couplings of axion-like particles within different scenarios. Contrary to WIMP searches, we used fiducial *electron* recoils as a potential axion signal. The collected data provide both a reasonably large exposure of up to 448 kg.d, and a good energy resolution of 0.8 keV FWHM at low energy. In addition, the remarkable rejection of near-surface events provided by the ID design, primarily used to reject surface beta radioactivity in WIMP searches, also allows the rejection of additional low-energy gamma-rays of external origin. This rejection provides an average background as low as 0.3 counts/kg/d/keV at 12 keV.

We set new limits on ALP parameters for different scenarios, some of which provide the best bounds for direct axion searches. The 95% CL bound $g_{A\gamma} < 2.13 \text{ GeV}^{-1}$ derived from the

solar Primakoff channel constrains axion models in the mass range $\sim 1 - 100$ eV for hadronic axions. This constraint is complementary to helioscope bounds, which can currently only probe lower axion masses within these models. Remarkably, the model-independent bound on g_{Ae} obtained from the search for solar Compton-bremsstrahlung-RD axions reaches a better sensitivity than the more indirect bound derived from solar neutrino flux measurements [42]. Combining the results from all solar axion channels provides a wide model-dependent mass exclusion range, $0.91 \text{ eV} < m_A < 80 \text{ keV}$ within the DFSZ framework and $5.73 \text{ eV} < m_A < 40 \text{ keV}$ for KSVZ axions. This is a prominent result for a direct axion search from a single dataset.

We therefore demonstrated the potential of germanium bolometric detectors equipped with the ID design for future ALP searches. Improvements are expected with future setups, such as EDELWEISS-III and EURECA [48], thanks to both better energy resolution and larger exposures.

Acknowledgments

The help of the technical staff of the Laboratoire Souterrain de Modane and the participant laboratories is gratefully acknowledged. The EDELWEISS project is supported in part by the French Agence Nationale pour la Recherche (contract ANR-10-BLAN-0422-03) and P2IO Labex (Postdoc call 2012), the German ministry of science and education (BMBF) within the Verbundforschung Astroteilchenphysik (grant 05A11VK2), the Helmholtz Alliance for Astroparticle Physics (HAP) funded by the Initiative and Networking Fund of the Helmholtz Association, the Russian Foundation for Basic Research (Russia) and the Science and Technology Facilities Council (UK). We would like to thank also E. Ferrer-Ribas, I. G. Irastorza, B. Lakić and T. Papaevangelou for fruitful discussions.

References

- [1] R. D. Peccei and Helen R. Quinn, *Constraints Imposed by CP Conservation in the Presence of Instantons*, *Phys. Rev. D* **16** (1977) 1791.
- [2] S. Weinberg, *A New Light Boson?*, *Phys. Rev. Lett.* **40** (1978) 223.
- [3] F. Wilczek, *Problem of Strong p and t Invariance in the Presence of Instantons*, *Phys. Rev. Lett.* **40** (1978) 279.
- [4] J. E. Kim, *Weak Interaction Singlet and Strong CP Invariance*, *Phys. Lett.* **43** (1979) 103; M. A. Shifman et al., *Can Confinement Ensure Natural CP Invariance of Strong Interactions?*, *Nucl. Phys. B* **166** (1980) 493.
- [5] A. R. Zhitniskiy, *On possible suppression of the axion hadron interactions*, *Yad. Fiz.* **31** (1980) 497; M. Dine et al., *A Simple Solution to the Strong CP Problem with a Harmless Axion*, *Phys. Lett. B* **104** (1981) 199.
- [6] J. Beringer et al. (Particle Data Group), *Phys. Rev. D* **86**, (2012) 010001.
- [7] D. B. Kaplan, *Opening the Axion Window*, *Nucl. Phys. B* **260** (1985) 215.
- [8] M. Srednicki, *Axion Couplings to Matter. 1. CP Conserving Parts*, *Nucl. Phys. B* **260** (1985) 689.
- [9] Svrcek and Witten, *Axions in String Theory*, *JHEP* **0606** (2006) 051.
- [10] A. Broniatowski et al., *A new high-background-rejection dark matter Ge cryogenic detector*, *Phys. Lett. B* **681** (2009) 305.

- [11] S. Andriamonje et al. (CAST collaboration), *An improved limit on the axion-photon coupling from the CAST experiment*, *JCAP* **04** (2007) 010.
- [12] L. Di Lella et al., *Search for solar Kaluza-Klein axions in theories of low-scale quantum gravity*, *Phys. Rev. D* **62** (2000) 125011.
- [13] A. Serenelli et al., *New Solar Composition: The Problem With Solar Models Revisited*, *Astrophys. J.* **705** (2009) L123.
- [14] S. Moriyama, *A Proposal to search for a monochromatic component of solar axions using Fe-57*, *Phys. Rev. Lett.* **75** no. 18 (1995) 3222.
- [15] W. C. Haxton and K. Y. Lee, *Red giant evolution, metallicity and new bounds on hadronic axions*, *Phys. Rev. Lett.* **66** no. 20 (1991) 2557.
- [16] V. Mateu and A. Pich, *V(us) Determination from Hyperon Semileptonic Decays*, *J. High Energy Phys.* **10** (2005) 041.
- [17] D. Adams et al. (Spin Muon Collaboration), *Spin structure of the proton from polarized inclusive deep inelastic muon - proton scattering*, *Phys. Rev. D* **56** (1997) no. 9, 5330-5358.
- [18] G. Altarelli et al., *Determination of the Bjorken sum and strong coupling from polarized structure functions*, *Nucl. Phys. B* **496** (1997) 337.
- [19] F. T. Avignone, *Search for axions from the 1115-keV transition of Cu-65*, *Phys. Rev. D* **37** (1988) 618.
- [20] S. Andriamonje et al. (CAST collaboration), *Search for 14.4-keV solar axions emitted in the M1-transition of Fe-57 nuclei with CAST*, *JCAP* **12** (2009) 002.
- [21] F. Alessandria et al., *Search for 14.4 keV solar axions from M1 transition of Fe-57 with CUORE crystals*, *JCAP* **05** (2013) 007.
- [22] K. Barth et al., *CAST constraints on the axion-electron coupling*, *JCAP* **05** (2013) 010.
- [23] R. Bernabei et al., *Investigating pseudoscalar and scalar dark matter*, *Int. J. Mod. Phys. A* **21** (2006) 1445.
- [24] R.J. Creswick et al., *Theory for the direct detection of solar axions by coherent Primakoff conversion in germanium detectors*, *Phys. Lett. B* **427** (1998) 235.
- [25] A. Derevianko et al., *Axio-electric effect*, *Phys. Rev. D* **82** (2010) 065006.
- [26] M. Pospelov et al., *Bosonic super-WIMPs as keV-scale dark matter*, *Phys. Rev. D* **78** (2008) 115012.
- [27] <http://physics.nist.gov/PhysRefData/Xcom/html/xcom1.html>
- [28] E. Armengaud et al., *First results of the EDELWEISS-II WIMP search using Ge cryogenic detectors with interleaved electrodes*, *Phys. Lett. B* **687** (2010) 294.
- [29] E. Armengaud et al., *Final results of the EDELWEISS-II WIMP search using a 4-kg array of cryogenic germanium detectors with interleaved electrodes*, *Phys. Lett. B* **702** (2011) 329.
- [30] E. Armengaud et al., *Search for low-mass WIMPs with EDELWEISS-II heat-and-ionization detectors*, *Phys. Rev. D* **86**, (2012) 051701(R).
- [31] B. Schmidt et al. (EDELWEISS Collaboration), *Muon-induced background in the EDELWEISS dark matter search*, *Astroparticle Phys.* **44** (2013) 28.
- [32] S. Cebrian et al., *Prospects of solar axion searches with crystal detectors*, *Astrop. Phys.*, **10** (1999) 397.
- [33] E. Armengaud et al., *Background studies for the EDELWEISS dark matter experiment*, Accepted to be published in *Astroparticle Physics*, arXiv:1305.3628.

- [34] F. T. Avignone III et al., *Experimental search for solar axions via coherent Primakoff conversion in a germanium spectrometer*, *Phys. Rev. Lett.* **81** (1998) 5068.
- [35] A. Morales et al., *Particle dark matter and solar axion searches with a small germanium detector at the Canfranc Underground Laboratory*, *Astropart. Phys.* **16** (2002) 325.
- [36] Z. Ahmed et al. (CDMS Collaboration), *Search for Axions with the CDMS Experiment*, *Phys. Rev. Lett.* **103** (2009) 141802.
- [37] R. Bernabei et al., *Search for solar axions by Primakoff effect in NaI crystals*, *Phys.Lett.* **B 515** (2001) 6.
- [38] E. Arik et al. (CAST Collab.), *CAST search for sub-eV mass solar axions with ^3He buffer gas*, *Phys. Rev. Lett.* **107** (2011) 261302.
- [39] G.G. Raffelt, *Stars as Laboratories for Fundamental Physics*, University of Chicago Press, Chicago (1996).
- [40] G. J. Feldman and R. D. Cousins, *A Unified Approach to the Classical Statistical Analysis of Small Signals*, *Phys.Rev. D*, **57** (1998) 3873.
- [41] C. E. Aalseth et al. (CoGeNT Collaboration), *Experimental constraints on a dark matter origin for the DAMA annual modulation effect*, *Phys. Rev. Lett.* **101** (2008) 251301 [Erratum-ibid.102 (2009) 109903].
- [42] P. Gondolo and G. G. Raffelt, *Solar neutrino limit on axions and keV-mass bosons*, *Phys. Rev. D* **79** (2009) 107301.
- [43] A. V. Derbin, *Search for solar axions produced by Compton process and bremsstrahlung using axioelectric effect*, *JETP Lett.* **95** (2012) 379.
- [44] K. Abe, K. Hieda, K. Hiraide, S. Hirano, Y. Kishimoto, K. Kobayashi, S. Moriyama and K. Nakagawa et al., *Search for solar axions in XMASS, a large liquid-xenon detector* arXiv:1212.6153v2 [astro-ph.CO]
- [45] A. V. Derbin, A. S. Kayunov, V. N. Muratova, D.A. Semenov, E.V. Unzhakov, *Search for Solar Axions Produced in the $p + d \rightarrow ^3\text{He} + A$ Reaction*, *Phys. Rev. D* **83** (2011) 023505.
- [46] G. Bellini et al. (Borexino Collaboration), *Search for Solar Axions Produced in $p(d,^3\text{He})A$ Reaction with Borexino Detector*, *Phys. Rev D* **85** (2012) 092003.
- [47] G. G. Raffelt, *Astrophysical axion bounds*, *Lect. Notes Phys.* **741** (2008) 51.
- [48] H. Kraus et al., *EURECA: The European future of dark matter searches with cryogenic detectors*, *Nucl. Phys.* **B**, (Proc. Suppl.) 173 (2007) 168.